

# The conduit equation: Hyperbolic approximation and generalized Riemann problem

Sergey Gavriluk<sup>a,\*</sup>, Boniface Nkonga<sup>b</sup>, Keh-Ming Shyue<sup>c</sup>

<sup>a</sup> Aix Marseille University, CNRS, IUSTI, UMR 7343, Marseille, France

<sup>b</sup> Université de Nice Sophia-Antipolis, CNRS UMR 7351, Laboratoire J.A.Dieudonné, Parc Valrose, 06108 Nice Cedex 2, France

<sup>c</sup> Institute of Applied Mathematical Sciences, National Taiwan University, Taipei 106, Taiwan

## ARTICLE INFO

MSC:  
35L40  
35Q35  
35Q74

## ABSTRACT

The conduit equation is a dispersive non-integrable scalar equation modeling the flow of a low-viscous buoyant fluid embedded in a highly viscous fluid matrix. This equation can be written in a particular form reminiscent of the famous Godunov form proposed in 1961 for the Euler equations of compressible fluids. We propose a hyperbolic approximation of the conduit equation by retaining the Godunov-type structure. The comparison of solutions to the conduit equation and those to the approximate hyperbolic system is performed: the wave fission of a large initial perturbation of a rectangular or Gaussian form. The results are in good agreement. New generalized solutions to the conduit equation composed of a finite set of waves of the same period and linked with a constant solution by generalized Rankine-Hugoniot relations are discovered. Such multi-hump structures interact with each other almost as solitary waves: they collide, merge, and reconstruct after the interaction. This partly indicates the stability of such multi-hump solutions under small perturbations. The exact and approximate hyperbolic system describes such an interaction with good accuracy.

## 1. Introduction

Consider the *conduit equation*:

$$u_t + (u^2 + u_x u_t - uu_{tx})_x = 0, \quad (1)$$

involving one dependent variable  $u(t, x)$  and two independent variables  $t$  (time) and  $x$  (space coordinate). Physically, the equation (1) represents the mass conservation law written in dimensionless variables for the magnitude  $u(t, x)$  of the non-dimensional circular cross-section of a low-viscosity buoyant fluid embedded in a highly viscous fluid at rest (cf. [29,22–24,27,26,25]). Hence, only positive solutions  $u(t, x)$  are physically admissible. Another conservative form which, *a priori*, has no physical meaning can be found for the conduit equation:

$$\left( \frac{1}{u} + \frac{u_{xx}}{u} \right)_t - (2 \ln(u))_x = 0. \quad (2)$$

\* Corresponding author.

E-mail addresses: [sergey.gavriluk@univ-amu.fr](mailto:sergey.gavriluk@univ-amu.fr) (S. Gavriluk), [Boniface.Nkonga@unice.fr](mailto:Boniface.Nkonga@unice.fr) (B. Nkonga), [shyue@ntu.edu.tw](mailto:shyue@ntu.edu.tw) (K.-M. Shyue).

Its mathematical importance will be shown later. The dispersion relation for the conduit equation linearized on the solution  $u = u_0 = \text{const} > 0$  can be written as

$$c_p = \frac{2u_0}{1 + u_0 k^2}, \tag{3}$$

where  $k$  is the wave number, and  $c_p$  is the corresponding phase velocity. It has the same dispersive properties as the Benjamin-Bona-Mahony (BBM) equation [1]. The derivation of the modulation equations to the conduit equation and their stability study for small amplitude waves has been performed in [26,16].

In [8,6,4,10,2,32], a general method of hyperbolic regularization of dispersive equations that are the Euler-Lagrange equations for a “master” Lagrangian has been proposed: the original high order derivative dispersive equations were approximated by a first order hyperbolic system of the Euler-Lagrange equations for a one or two-parameter family of “extended” Lagrangians. The “master” Lagrangian is obtained from the “extended” Lagrangian in some limit. Thus, the variational structure of the governing equations was conserved. In a particular case of long gravity surface waves described by the Serre-Green-Naghdi equations, the method of “extended Lagrangian” was mathematically justified in [7]. The advantage of such an approach is obvious: one can use the full range of finite volume methods developed for hyperbolic equations for dispersive equations. Furthermore, some non-linear dispersive equations admit shock-type solutions: the dispersion cannot always prevent the formation of such singularities [11,9]. A hyperbolic approximation is therefore a natural option for dealing with strong discontinuities.

Despite a large number of works on the conduit equation, unlike the almost similar BBM equation (at least in the linear limit), neither other linearly independent conservation laws for this equation, nor the existence of a Lagrangian allows this equation to be considered as the Euler-Lagrange equation, are known [16]. Having in mind to approximate the conduit equation by a system of hyperbolic equations, we then ask the following question: what is the mathematical structure (different from a classical variational structure) of the conduit equation, and should it be retained when a system of hyperbolic equations approximates the equation?

In this paper, we will exhibit such a structure and will formulate an approximating hyperbolic system of equations conserving this structure. Comparing numerical solutions to the exact conduit equation and to its “structure conserving” hyperbolic approximation shows very good convergence results.

## 2. Mathematical structure of the conduit equation

In 1961 [13] S.K. Godunov proposed the following abstract form of a system of conservation laws for the vector variable  $\mathbf{v} = (v_1, v_2, \dots, v_n)^T$ :

$$\left( \frac{\partial L^0(\mathbf{v})}{\partial \mathbf{v}} \right)_t + \sum_{i=1}^m \left( \frac{\partial L^i(\mathbf{v})}{\partial \mathbf{v}} \right)_{x_i} = 0, \tag{4}$$

with given functions (potentials)  $L^i(\mathbf{v})$ ,  $i = 0, 1, \dots, m$ . This system admits an additional conservation law

$$\left( \frac{\partial L^0(\mathbf{v})}{\partial \mathbf{v}} \cdot \mathbf{v} - L^0(\mathbf{v}) \right)_t + \sum_{i=1}^m \left( \frac{\partial L^i}{\partial \mathbf{v}} \cdot \mathbf{v} - L^i \right)_{x_i} = 0. \tag{5}$$

If the Hessian matrix of  $L^0$  is positive definite, the equations can be written in the symmetric form of Friedrichs. Denoting the variable  $t$  by  $x_0$ , we can rewrite the system (4) and its consequence (5) in a compact form:

$$\frac{\partial}{\partial x^\beta} \left( \frac{\partial L^\beta}{\partial v^\alpha} \right) = 0, \quad \frac{\partial E^\beta}{\partial x^\beta} = 0, \quad E^\beta = v^\alpha \frac{\partial L^\beta}{\partial v^\alpha} - L^\beta, \tag{6}$$

with  $\beta = 0, 1, \dots, m$ ,  $\alpha = 1, 2, \dots, n$ . Here the summation is taken over repeated indexes. A number of reversible models of continuum mechanics can be written in Godunov’s form (6) [14].

A generalization of such a class of models with multiple examples from the reversible continuum mechanics was proposed in [12], with potentials  $L^\beta$  depending not only on unknowns but also on their first derivatives. More precisely, let us denote  $v_{,\gamma}^\alpha = \frac{\partial v^\alpha}{\partial x^\gamma}$ . Consider functions  $L^\beta(v^\alpha, v_{,\gamma}^\alpha)$  (we will use the same notations as for the old potentials  $L^\beta$  depending only on  $v^\beta$ ) and a conservative system in the form

$$\frac{\partial}{\partial x^\beta} \left( \frac{\delta L^\beta}{\delta v^\alpha} \right) = 0. \tag{7}$$

Here we used conventional notations for the variational derivatives:

$$\frac{\delta L^\beta}{\delta v^\alpha} = \frac{\partial L^\beta}{\partial v^\alpha} - \frac{\partial}{\partial x^\gamma} \left( \frac{\partial L^\beta}{\partial v_{,\gamma}^\alpha} \right).$$

Equations (7) also admit an additional conservation law

$$\frac{\partial E^\beta}{\partial x^\beta} = 0, \quad E^\beta = v^\alpha \frac{\delta L^\beta}{\delta v^\alpha} - L^\beta + v_{,\gamma}^\alpha \frac{\partial L^\beta}{\partial v_{,\gamma}^\alpha}. \tag{8}$$

Let us rewrite the conduit equation in the form (7). For this, we will use the conservative form (2) with  $x^0 = t$  and  $x^1 = x$ . Let us consider the change of variables

$$u = \sqrt{1 + 2v} \tag{9}$$

and potentials  $L(v, v_x)$  and  $M(v)$  (instead of generic potentials  $L^0$  and  $L^1$ ) defined as:

$$L(v, v_x) = \sqrt{1 + 2v} - \frac{v_x^2}{2(1 + 2v)}, \quad M(v) = -\frac{1}{2}(1 + 2v)(\ln(1 + 2v) - 1). \tag{10}$$

Then, one obtains:

$$\frac{\delta L}{\delta v} = \frac{1}{\sqrt{1 + 2v}} + \frac{v_{xx}}{1 + 2v} - \frac{v_x^2}{(1 + 2v)^2} = \frac{1 + u_{xx}}{u} = \frac{1}{u} + \frac{u_{xx}}{u}, \tag{11}$$

$$\frac{\partial M(v)}{\partial v} = -\ln(1 + 2v) = -2 \ln(u). \tag{12}$$

Hence, the equation (2) is written of the form (7):

$$\left( \frac{\delta L(v, v_x)}{\delta v} \right)_t + \left( \frac{\partial M(v)}{\partial v} \right)_x = 0. \tag{13}$$

The equation (13) admits an additional conservation law:

$$\left( v \frac{\delta L}{\delta v} - L \right)_t + \left( v_t \frac{\partial L}{\partial v_x} + v \frac{\partial M}{\partial v} - M \right)_x = 0. \tag{14}$$

Unfortunately, it is not a new conservation law, but just a linear combination of (1) and (2). The equations (13) also admit a symmetric form. Indeed, consider the partial Legendre transform of  $L$ :

$$L^*(v, w) = wv_x - L(v, v_x), \quad \text{where } w = \frac{\partial L}{\partial v_x}. \tag{15}$$

It implies, by using the implicit function theorem,

$$\frac{\partial L^*}{\partial v} = -\frac{\partial L}{\partial v} \quad \text{and} \quad \frac{\partial L^*}{\partial w} = v_x. \tag{16}$$

One has

$$\left( \frac{\partial L^*}{\partial v} \right)_t - \left( \frac{\partial M}{\partial v} \right)_x + w_{tx} = 0, \quad \left( \frac{\partial L^*}{\partial w} \right)_t - v_{tx} = 0. \tag{17}$$

It implies the following symmetric form:

$$AU_t + BU_x + CU_{tx} = 0, \quad \text{with } U = \begin{pmatrix} v \\ w \end{pmatrix}, \tag{18}$$

and

$$A = A^T = \begin{pmatrix} \frac{\partial^2 L^*}{\partial v^2} & \frac{\partial^2 L^*}{\partial v \partial w} \\ \frac{\partial^2 L^*}{\partial v \partial w} & \frac{\partial^2 L^*}{\partial w^2} \end{pmatrix}, \quad B = B^T = \begin{pmatrix} \frac{\partial^2 M}{\partial v^2} & 0 \\ 0 & 0 \end{pmatrix}, \quad C = -C^T = \begin{pmatrix} 0 & 1 \\ -1 & 0 \end{pmatrix}.$$

### 3. Extended hyperbolic system

The idea of the hyperbolic approximation of the equation (1) is to replace it by an “extended” parametric family of reversible hyperbolic systems also having the Godunov-type form (7). The word “extended” means that the governing equations contain an extra unknown  $z(t, x)$  which is asymptotically close to the unknown  $u(t, x)$  when parameters of the model go to infinity. Such a “penalization” method was already used in [8,6,4,10,2,3] for mathematical models admitting a variational formulation. The “extended” system of equations was obtained as the Euler-Lagrange equations for an “extended” Lagrangian. Equation (13) does not correspond to any Euler–Lagrange equation. Indeed, it involves two potentials,  $L$  and  $M$ , while the Euler-Lagrange equations are written in terms of a single potential (Lagrange function). By doing so, we expect a better approximation of the conduit equation by the corresponding hyperbolic system of equations.

Consider a two-parameter family of potentials

$$\mathcal{L}(v, z, z_x, z_t) = \sqrt{1 + 2v} + \frac{z_t^2}{2c^2} - \frac{z_x^2}{2} - \frac{\lambda}{2} \left( z - \sqrt{1 + 2v} \right)^2, \tag{19}$$

where  $\lambda$  and  $c$  are large parameters. Let us replace the equation (13) by a system of equations for two unknowns  $v$  and  $z$ :

$$\left(\frac{\partial \mathcal{L}}{\partial v}\right)_t + \left(\frac{\partial M}{\partial v}\right)_x = 0 \quad \text{and} \quad \frac{\delta \mathcal{L}}{\delta z} = 0, \tag{20}$$

with

$$\frac{\delta \mathcal{L}}{\delta z} = \frac{\partial \mathcal{L}}{\partial z} - \left(\frac{\partial \mathcal{L}}{\partial z_t}\right)_t - \left(\frac{\partial \mathcal{L}}{\partial z_x}\right)_x.$$

It admits the conservation law:

$$\left(z_t \frac{\partial \mathcal{L}}{\partial z_t} + v \frac{\partial \mathcal{L}}{\partial v} - \mathcal{L}\right)_t + \left(z_t \frac{\partial \mathcal{L}}{\partial z_x} + v \frac{\partial M}{\partial v} - M\right)_x = 0. \tag{21}$$

Indeed, straightforward computations give the identity

$$\begin{aligned} \left(z_t \frac{\partial \mathcal{L}}{\partial z_t} + v \frac{\partial \mathcal{L}}{\partial v} - \mathcal{L}\right)_t + \left(z_t \frac{\partial \mathcal{L}}{\partial z_x} + v \frac{\partial M}{\partial v} - M\right)_x = \\ v \left(\left(\frac{\partial \mathcal{L}}{\partial v}\right)_t + \left(\frac{\partial M}{\partial v}\right)_x\right) - z_t \frac{\delta \mathcal{L}}{\delta z} = 0. \end{aligned}$$

Since  $M$  is a function of  $v$  only, and  $\mathcal{L}$  does not depend on space and time derivatives of  $v$ , (20) can be rewritten in the form

$$\left(\frac{\partial \mathcal{L}}{\partial v}\right)_t + \left(\frac{\partial M}{\partial v}\right)_x = 0 \quad \text{and} \quad \left(\frac{\delta \mathcal{L}}{\delta z}\right)_t + \left(\frac{\partial M}{\partial z}\right)_x = 0,$$

which is exactly the form (7) with (21) corresponding to (8).

Now we will write the equations (20) in explicit form by using the expressions for derivatives:

$$\frac{\partial \mathcal{L}}{\partial v} = \frac{1}{\sqrt{1+2v}} + \lambda \frac{z - \sqrt{1+2v}}{\sqrt{1+2v}}, \tag{22a}$$

$$\frac{\partial \mathcal{L}}{\partial z} = -\lambda(z - \sqrt{1+2v}), \tag{22b}$$

$$\frac{\partial \mathcal{L}}{\partial z_x} = -z_x, \tag{22c}$$

$$\frac{\partial \mathcal{L}}{\partial z_t} = \frac{z_t}{c^2}. \tag{22d}$$

The first equation of (20) becomes:

$$\left(\frac{1}{\sqrt{1+2v}} + \lambda \frac{z - \sqrt{1+2v}}{\sqrt{1+2v}}\right)_t - \frac{2}{1+2v} v_x = 0. \tag{23}$$

The second equation of (20) becomes:

$$-\frac{1}{c^2} z_{tt} + z_{xx} = \lambda(z - \sqrt{1+2v}). \tag{24}$$

Finally, we return back to  $u$ -variable ( $u = \sqrt{1+2v}$ ):

$$\left(\frac{1}{u} + \lambda \frac{z-u}{u}\right)_t - \frac{2u_x}{u} = 0, \quad -\frac{1}{c^2} z_{tt} + z_{xx} = \lambda(z-u). \tag{25}$$

Similar to the conduit equation, this system is reversible in the sense that it is invariant under the change of independent variables  $t \rightarrow -t, x \rightarrow -x$ . Its first order quasi-linear formulation can then be written as:

$$\left(\frac{1}{u} + \lambda \frac{z-u}{u}\right)_t - \frac{2u_x}{u} = 0, \tag{26a}$$

$$-\frac{1}{c} z_t + z_x = p, \tag{26b}$$

$$\frac{1}{c} p_t + p_x = \lambda(z-u). \tag{26c}$$

The eigenvalues are  $s_1 = -c, s_2 = 2u/(1 + \lambda z),$  and  $s_3 = c.$  The associated eigenvectors are

$$\mathbf{R}_1 = \begin{pmatrix} -2\lambda c/(2u + c(1 + \lambda z)) \\ 1 \\ 0 \end{pmatrix}, \quad \mathbf{R}_2 = \begin{pmatrix} 1 \\ 0 \\ 0 \end{pmatrix}, \quad \mathbf{R}_3 = \begin{pmatrix} 0 \\ 0 \\ 1 \end{pmatrix}.$$

For large enough  $c$  and  $\lambda,$  the equations are strictly hyperbolic. The initial conditions for (26) are:

$$u(0, x) = u_0(x), \quad z(0, x) = u_0(x), \quad p(0, x) = \frac{du_0(x)}{dx}. \tag{27}$$

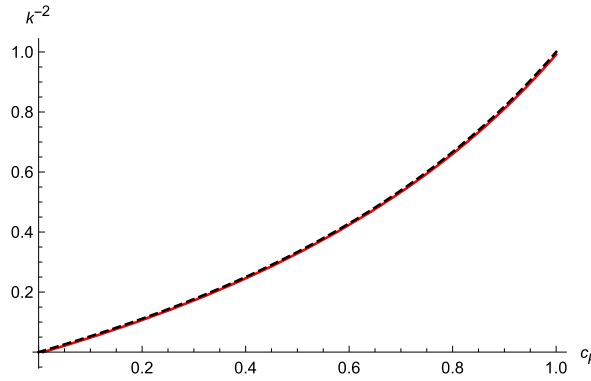


Fig. 1. Comparison of the exact dispersion relation for  $u_0 = 1$  (black dashed curve) and approximate one (red curve for  $c = 15$ ,  $\lambda = c^2 = 225$ ) is shown. (For interpretation of the colors in the figure(s), the reader is referred to the web version of this article.)

These are the conditions we used for the numerical tests in Section 7. In the following, we will take  $\lambda = c^2$ . The system (25) admits the conservation law (21) which is equivalent to the following one:

$$\left( \frac{z_t^2}{c^2} + z_x^2 + \lambda z^2 - u(1 + \lambda z) \right)_t - (u^2 + 2z_t z_x)_x = 0. \tag{28}$$

#### 4. Dispersion relation

The dispersion relation for the hyperbolic system (26) linearized on the solution  $u = u_0$ ,  $z = u_0$ ,  $p = 0$  is:

$$\frac{1}{k^2} = \frac{1 + \lambda u_0}{\lambda} \frac{(c_p^2/c^2 - 1)(c_p - 2u_0/(1 + \lambda u_0))}{c_p - 2u_0}. \tag{29}$$

For any wave number  $k$  the real root  $c_p$  approximating the exact dispersion relation (3) satisfies the inequality

$$\frac{2u_0}{1 + \lambda u_0} < c_p < 2u_0. \tag{30}$$

For large  $\lambda$  and  $c^2$  the approximate dispersion relation can be written as:

$$\frac{1}{k^2} = \frac{c_p u_0}{2u_0 - c_p} + \mathcal{O}\left(\frac{1}{\lambda} + \frac{1}{c^2}\right). \tag{31}$$

Fig. 1 shows the “quality” of the approximate dispersion relation (29). The asymptotic formula (31) suggests a natural choice of  $\lambda = c^2$  to pass to one parameter family of penalty functions  $\mathcal{L}(v, z, z_t, z_x)$  defined by (19).

#### 5. Periodic solutions

Periodic and solitary wave solutions to the conduit equation can be found, for example, in [29]. Here a quick overview of the solutions is given. Looking for traveling solutions to (2) depending only on  $\xi = x - Dt$ ,  $D = const > 0$  is the wave velocity, one obtains the ODE:

$$Du'' = (C - 1)u - 2u \ln(u) - D, \quad C = const, \tag{32}$$

admitting the first integral

$$Du'^2 = P(u) = Cu^2 - 2u^2 \ln(u) - 2Du - Q, \quad Q = const. \tag{33}$$

Here “prime” means the derivative with respect to  $\xi$ . Since  $u \ln(u)$  is convex for  $u > 0$ , the function  $P(u)$  has maximum two critical points for  $u > 0$ , and hence maximum three roots. In the last case we denote them  $u_i$ ,  $P(u_i) = 0$ ,  $i = 1, 2, 3$ ,  $0 < u_1 < u_2 < u_3$ . A typical behavior of  $P(u)$  is shown in Fig. 2. One can construct periodic solution oscillating between  $u_2$  (minimum of the wave amplitude) and  $u_3$  (maximum of the wave amplitude). The case  $u_1 = u_2$  gives the solitary wave solutions. The wave velocity  $D$ , and the constants  $C$  and  $Q$  are thus calculated from the linear system:

$$Cu_i^2 - 2u_i^2 \ln(u_i) - 2Du_i - Q = 0, \quad i = 1, 2, 3. \tag{34}$$

Its solution is unique if  $u_1 \neq u_2 \neq u_3$ . The wave length  $L$  and averaged over the wave length the periodic solution  $\bar{u}$  are given by the following expressions coming directly from (33):

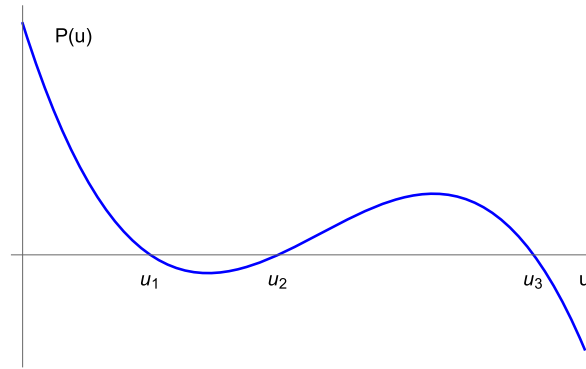


Fig. 2. A typical behavior of the function  $P(u)$  is shown. In a domain of parameters  $C, D > 0, Q < 0$  it has three roots  $0 < u_1 < u_2 < u_3$ . The periodic solution oscillates between  $u_2$  and  $u_3$ .

$$L = 2\sqrt{D} \int_{u_2}^{u_3} \frac{du}{\sqrt{P(u)}}, \quad \bar{u} = \frac{\int_{u_2}^{u_3} \frac{udu}{\sqrt{P(u)}}}{\int_{u_2}^{u_3} \frac{du}{\sqrt{P(u)}}}. \tag{35}$$

To study traveling wave solutions to (26), we will use the conservative form of equations:

$$\begin{aligned} \left(\frac{1}{u} + \lambda \frac{z-u}{u}\right)_t - (\ln(u^2))_x &= 0, \\ \left(\frac{z_t^2}{c^2} + z_x^2 + \lambda z^2 - u(1 + \lambda z)\right)_t - (u^2 + 2z_t z_x)_x &= 0. \end{aligned}$$

Using again the sign “prime” for the derivative with respect to the traveling wave coordinate  $\xi = x - Dt$ , one gets the following ODE system

$$-D \left(\frac{1}{u} + \lambda \frac{z-u}{u}\right) - \ln(u^2) = c_1, \tag{36a}$$

$$D \left(1 - \frac{D^2}{c^2}\right) z'^2 = D(\lambda z^2 - u(1 + \lambda z)) + u^2 + c_2, \tag{36b}$$

where  $c_i, i = 1, 2$  are constants. It can be reduced to only one equation for  $u$ . Indeed, one has

$$z = u - \frac{u}{D\lambda} \left(c_1 + \ln(u^2) + \frac{D}{u}\right), \tag{36c}$$

that yields

$$\frac{dz}{du} = 1 - \frac{1}{D\lambda} (c_1 + 2 + 2\ln(u)). \tag{36d}$$

Then the equation (36b) becomes

$$\begin{aligned} D \left(1 - \frac{D^2}{c^2}\right) \left(1 - \frac{1}{D\lambda} (c_1 + 2 + 2\ln(u))\right)^2 u'^2 = \\ \frac{u^2}{D\lambda} \left(D\lambda - c_1 - 2\ln(u) - \frac{D}{u}\right)^2 - D\lambda u^2 + c_1 u^2 + u^2 + 2u^2 \ln(u) + c_2. \end{aligned}$$

Finally, a compact form of this equation is:

$$u'^2 = \frac{F(u)}{G(u)}, \tag{37a}$$

where

$$F(u) = \frac{u^2}{D\lambda} \left(D\lambda - c_1 - 2\ln(u) - \frac{D}{u}\right)^2 + u^2 (1 + c_1 - D\lambda + 2\ln(u)) + c_2, \tag{37b}$$

$$G(u) = D \left(1 - \frac{D^2}{c^2}\right) \left(1 - \frac{1}{D\lambda} (c_1 + 2 + 2\ln(u))\right)^2. \tag{37c}$$

To find the solution of (37) numerically using an ODE solver, we need to determine the parameters  $c_1$ ,  $c_2$ , and  $D$  first. Given three constant states  $u_1$ ,  $u_2$ , and  $u_3$ ,  $0 < u_1 < u_2 < u_3$ , that are the equilibrium solutions of  $F(u)$ , this amounts solving the system of nonlinear equations:

$$F(u_1) = 0, \quad F(u_2) = 0, \quad F(u_3) = 0;$$

we do this by employing a quasi-Newton method (cf. [28]) using the coefficients from the periodic solution of the conduit equation as the initial guess, see (33), achieving the convergent results after 1 or 2 iterative steps, depending on the convergence tolerance. Once we get  $u$ , we may set  $z$  and  $p = \left(1 - \frac{D}{c}\right) z'$  based on (36c) and (36d), respectively.

### 6. Numerical methods

As in [8,10], we use a fractional-step approach for the numerical resolution of the hyperbolic conduit system: at each time step, we alternate between by solving the homogeneous (hyperbolic) part of the system (26)

$$\begin{pmatrix} 1/u + \lambda(z-u)/u \\ -z/c \\ p/c \end{pmatrix}_t + \begin{pmatrix} -\ln(u^2) \\ z \\ p \end{pmatrix}_x = 0 \tag{38a}$$

over a time step  $\Delta t$ , and the ODEs

$$\begin{pmatrix} 1/u + \lambda(z-u)/u \\ -z/c \\ p/c \end{pmatrix}_t = \begin{pmatrix} 0 \\ p \\ \lambda(z-u) \end{pmatrix} \tag{38b}$$

using the initial data from the previous step and the same time step. Here, the numerical approach we employed for solving (38a) is the same as for the conduit equation, see Appendix A. To update the solution of the ODEs (38b), we need to solve the linear second-order ODE:

$$z_{tt} + \frac{\lambda c^2 E_0}{E_0 + \lambda} z = \frac{\lambda c^2}{E_0 + \lambda} \tag{39a}$$

with the initial conditions

$$\left(\frac{1}{u} + \lambda \frac{z-u}{u}\right)\Big|_{t=0} = E_0, \quad z(0) = z_0, \quad p(0) = p_0. \tag{39b}$$

If  $E_0 > 0$ , its exact solution is:

$$z = \frac{1}{E_0} \left( 1 + (E_0 z_0 - 1) \cos(\omega t) - \frac{c p_0 E_0}{\omega} \sin(\omega t) \right), \tag{40a}$$

where  $\omega^2 = \lambda c^2 E_0 / (E_0 + \lambda)$ . We then have

$$p = -\frac{1}{c} z_t = p_0 \cos(\omega t) + \frac{\omega (E_0 z_0 - 1)}{c E_0} \sin(\omega t). \tag{40b}$$

If  $E_0 < 0$  ( $E_0 + \lambda > 0$  for large  $\lambda$ ), we find the exact solution:

$$z = \frac{1}{2E_0} \left( 2 + \left(E_0 z_0 - 1 - \frac{c p_0 E_0}{\mu}\right) e^{\mu t} + \left(E_0 z_0 - 1 + \frac{c p_0 E_0}{\mu}\right) \exp^{-\mu t} \right), \tag{40c}$$

$$p = -\frac{1}{c} z_t = -\frac{\mu}{2c E_0} \left( \left(E_0 z_0 - 1 - \frac{c p_0 E_0}{\mu}\right) e^{\mu t} - \left(E_0 z_0 - 1 + \frac{c p_0 E_0}{\mu}\right) \exp^{-\mu t} \right), \tag{40d}$$

where  $\mu^2 = -\lambda c^2 E_0 / (E_0 + \lambda)$ . Recall that  $E_0$ ,  $z_0$  and  $p_0$  are the solution of the homogeneous system (38a).

### 7. Numerical tests

For the tests in this section, we take a uniform mesh size  $\Delta x = 0.05$ , and a time step  $\Delta t$  determined from the Courant-Friedrich-Lewy (CFL) condition for the stability of the hyperbolic solver. The homogeneous Neumann boundary condition was employed on the left and right of the boundaries during the computations. The CFL number for all computations was 0.5. For comparison, we will present results obtained using four different schemes for the homogeneous system (38a): MUSCL, WENO3, WENO5, and BVD35. (see Appendix A for the details). The ODEs (38b) is solved using the exact solution (40) in all cases.

#### 7.1. Box test

Our first test is an example studied in [25] for solitary wave fission of a large disturbance in a viscous fluid conduit. In this test, the initial condition for the conduit equation is the box:

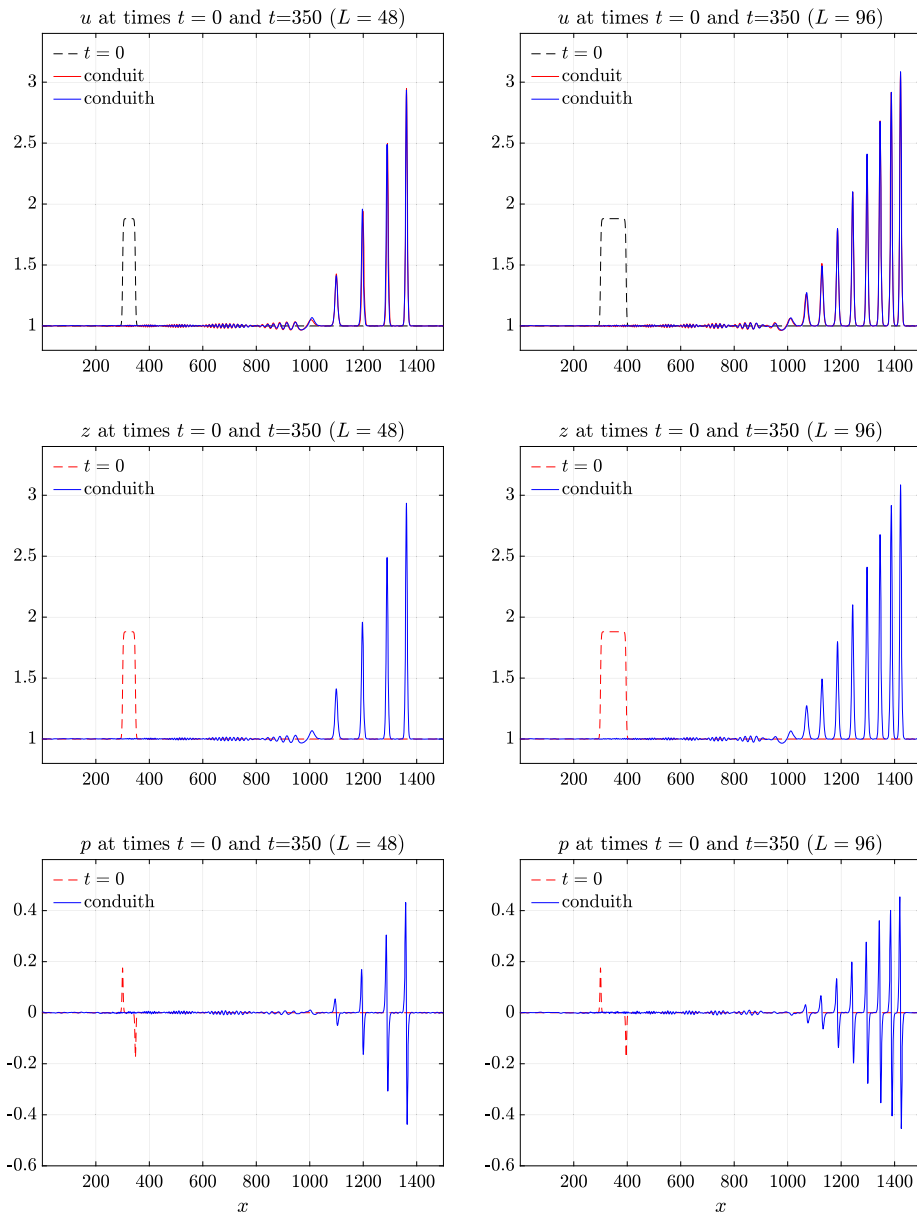


Fig. 3. Numerical results for the box test. Snapshots of solutions are obtained using BVD35 case of the method are shown at time  $t = 350$  for  $L = 48$  and  $L = 96$ . In both cases, parameter values  $c = 30$  and  $\lambda = 900$  were used in the computations. The blue line legend “conduith” means the results obtained using the hyperbolic approximation of the conduit equation, while the red line legend “conduit” is for the exact conduit equation.

$$u(0, x) = 1 + \frac{\alpha}{2} \left( \tanh \left( \frac{x - x_0}{\beta} \right) - \tanh \left( \frac{x - x_0 - L}{\beta} \right) \right), \tag{41}$$

where  $\alpha = 0.88$ ,  $\beta = 2.5$ , and  $x_0 = 300$  for  $x \in [0, 1500]$ .

For the hyperbolic model, the parameter values we set for  $c$  and  $\lambda$  are 30 and 900, respectively.

Fig. 3 shows numerical results for  $L = 48$  and  $96$  at time  $t = 350$  obtained using BVD35 case of the algorithm, observing good agreement of the state variable  $u$  between the conduit equation and its hyperbolic variant. In addition, we observe the similar solution structure between  $u$  and  $z$  which confirms the validity of our formal approach. For comparison, we repeat the computations using MUSCL, WENO3, and WENO5 cases. In Fig. 4 we show snapshots of the state variable  $u$  at time  $t = 350$  only partially in the region  $x \in [1000, 1500]$  (for completeness, the BVD35 results are included). It is clear that among them WENO5 and BVD35 give better solutions than WENO3 and MUSCL. For the MUSCL case, in particular, it is surprising to see the nonconvergence on the phase and amplitude for the foregoing solitary waves; this may mean that the third-order truncation (dispersive) error is too large for this problem, when discretizing the hyperbolic conduit equation based on the MUSCL approach.

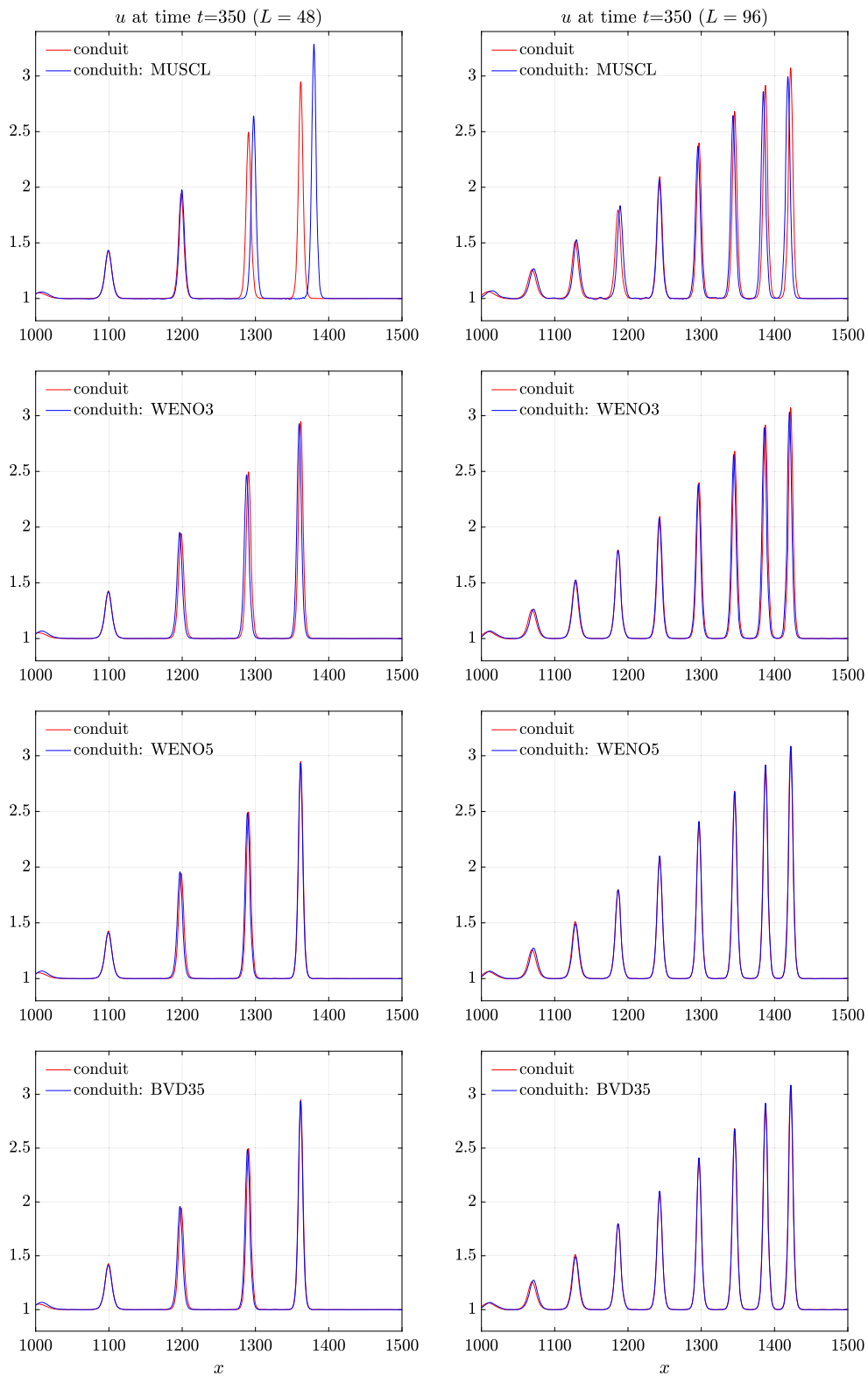


Fig. 4. Numerical methods comparison for the box test. Snapshots of the state variable  $u$  obtained using four different hyperbolic solvers are shown at time  $t = 350$  in the case of  $L = 48$  and  $L = 96$ ; only partial solutions in the region  $x \in [1000, 1500]$  are shown. In both cases, parameter values  $c = 30$  and  $\lambda = 900$  were used in the computations.

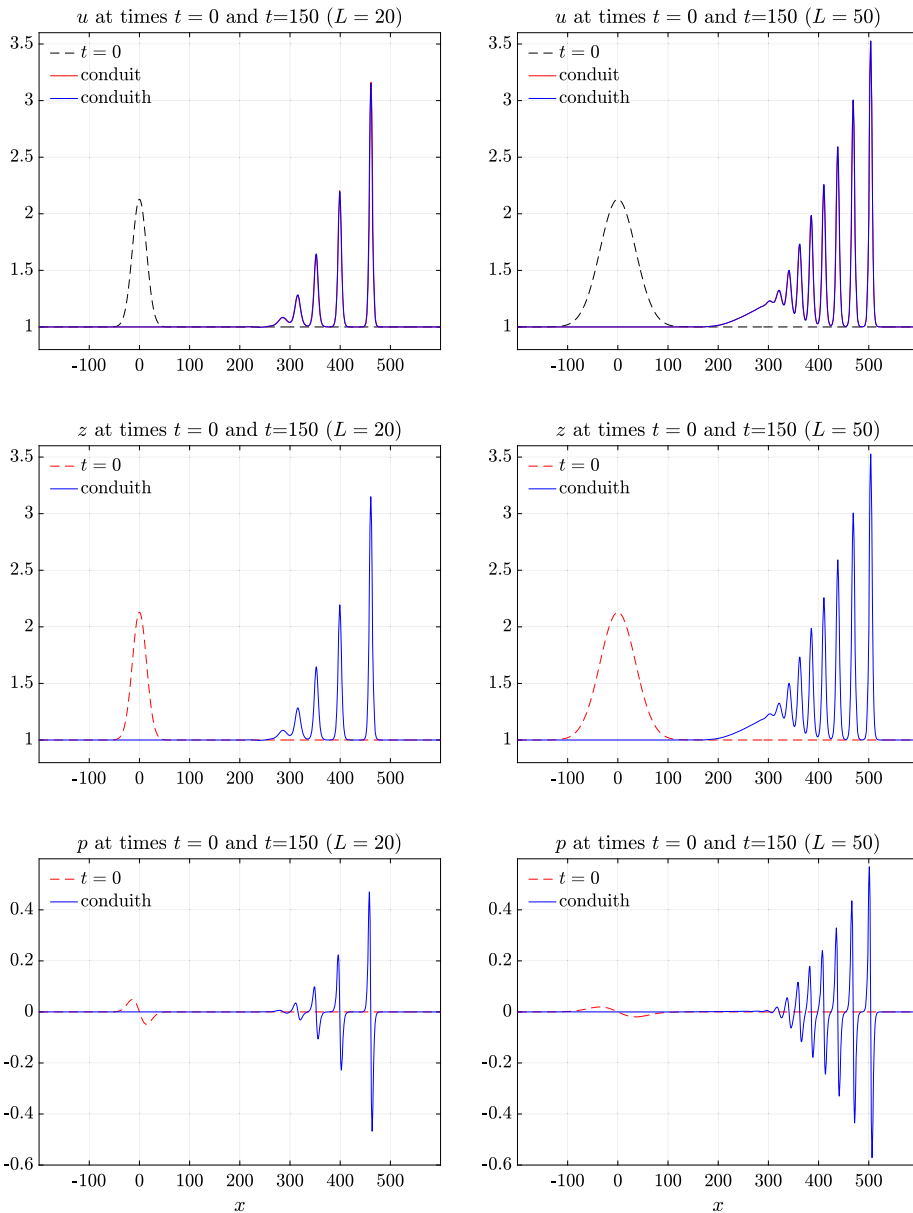


Fig. 5. Numerical results for the Gaussian test. Snapshots of solution obtained using BVD35 case of the method are shown at time  $t = 150$  for  $L = 20$  and  $L = 50$ . In both cases, parameter values  $c = 30$  and  $\lambda = 900$  were used in the computations.

### 7.2. Gaussian test

Our second test is an example studied in [10] for the BBM equation. In this test, for the conduit equation, we take the Gaussian profile:

$$u(0, x) = 1 + \frac{2}{\sqrt{\pi}} \exp(-x^2/L^2) \tag{42}$$

for  $x \in [-200, 600]$ . For the hyperbolic model, we use the same initialization procedure as before under (42), and the same parameter values for  $c$  and  $\lambda$  during the computations.

Fig. 5 shows numerical results in the case of  $L = 20$  and  $50$  at time  $t = 150$  obtained using BVD35 case of the algorithm. We again observe good agreement of the state variable  $u$  between the conduit equation and its hyperbolic variant, and also the same solution behavior between  $u$  and  $z$ . As in the previous test, we perform the computations using MUSCL, WENO3, and WENO5 cases also, and show numerical results in Fig. 6; only the partial solutions in the region  $x \in [200, 600]$  are shown. We find sensible good agreement of the solutions, even in the MUSCL case.

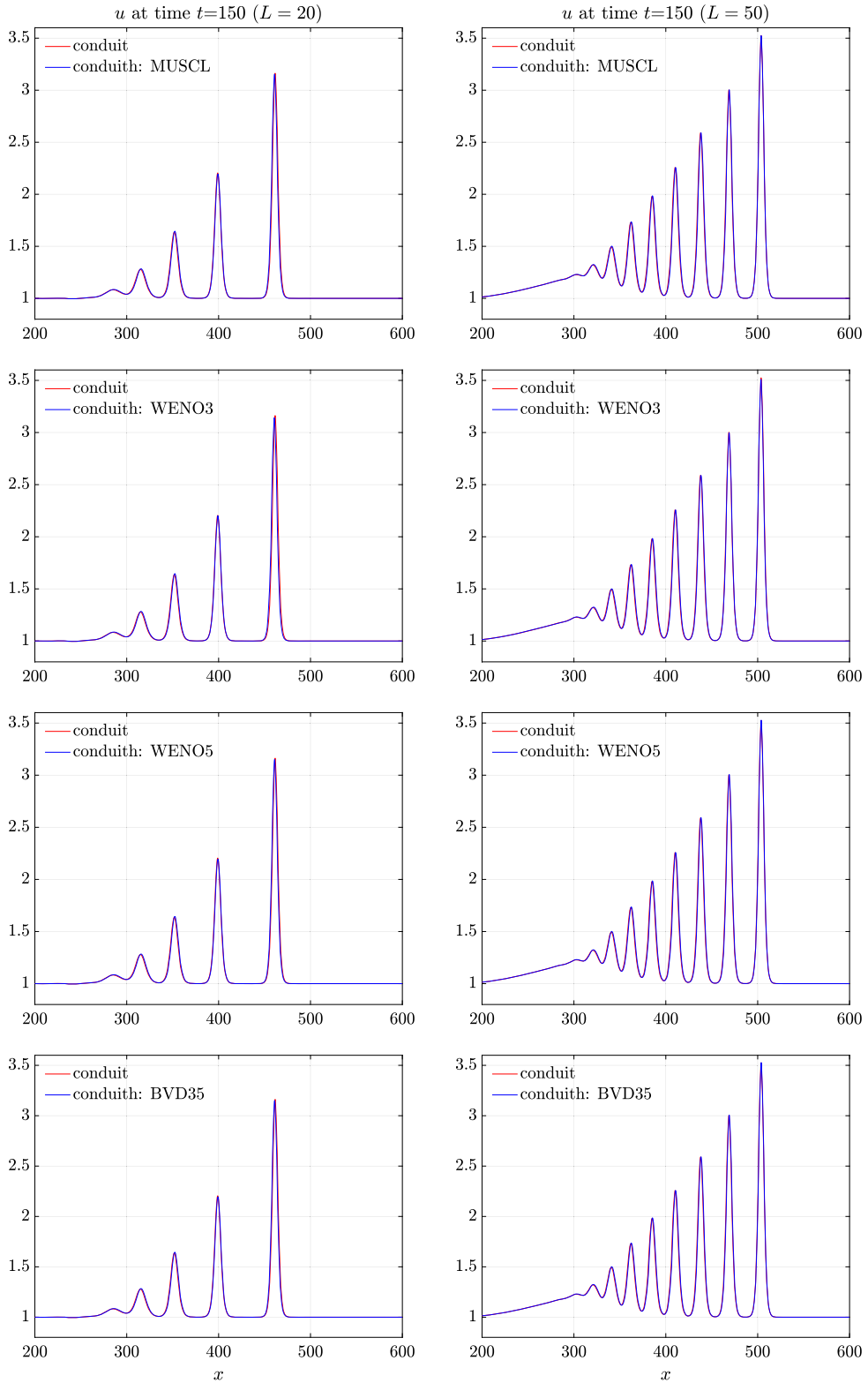


Fig. 6. Numerical methods comparison for the Gaussian test. Snapshots of the state variable  $u$  obtained using four different hyperbolic solvers are shown at time  $t = 150$  for  $L = 20$  and  $L = 50$ ; only the partial solutions in the region  $x \in [200, 600]$  are shown. In both cases, parameter values  $c = 30$  and  $\lambda = 900$  were used in the computations.

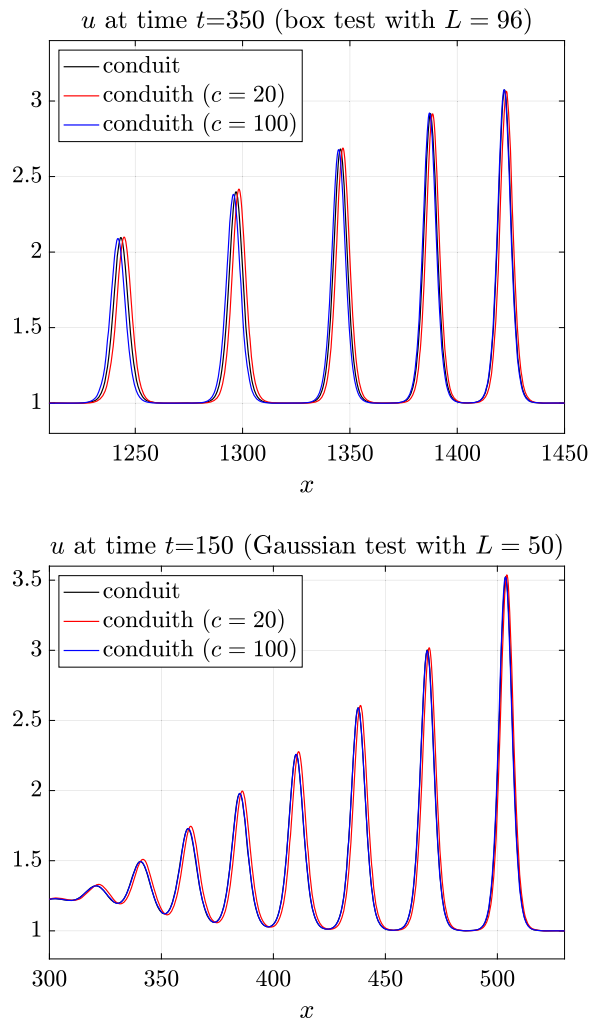


Fig. 7. A parameter study of the solutions on  $c$  and  $\lambda = c^2$  for the hyperbolic model. On the first row, the solutions are for the box test in the case of  $L = 96$  at time  $t = 350$ , and on the second row, the solutions are for the Gaussian test in the case of  $L = 50$  at time  $t = 150$ ; only the snapshots of the state variable  $u$  are shown together with the conduit solution. In both cases, we used parameter values  $c = 20$  and  $c = 100$  in the computations.

**Table 1**  
The CPU time (sec) taken for the numerical results shown in Fig. 7.

	conduit	hyperbolic model	
		$c = 20$	$c = 100$
box test	1021.528	3057.535	14572.31
Gaussian test	247.996	1238.719	6150.387

### 7.3. Parameter study

To end, we show the convergence of the hyperbolic conduit solution to the conduit one. For this, we perform a parameter study on  $c$  and  $\lambda = c^2$  for  $c = 20$  and  $100$ . In Fig. 7, the solutions of  $u$  for the box test in the case of  $L = 96$  and the Gaussian test in the case of  $L = 50$  are shown at times  $t = 350$  (the first row) and  $t = 150$  (the second row), respectively. Here, for clarity, only the partial solutions in the region  $x \in [1210, 1450]$  and  $x \in [300, 530]$  are drawn. It is clear that the solution is more accurate when a larger parameter is used in the computations. Table 1 gives the timing study in CPU (sec) for the results shown in Fig. 7, where the tests were performed in a Mac mini M2 Pro with 32GB RAM by using the BVD35 scheme. We observe the higher computational cost when the hyperbolic model (26) is used as compared to the dispersive conduit equation (2).

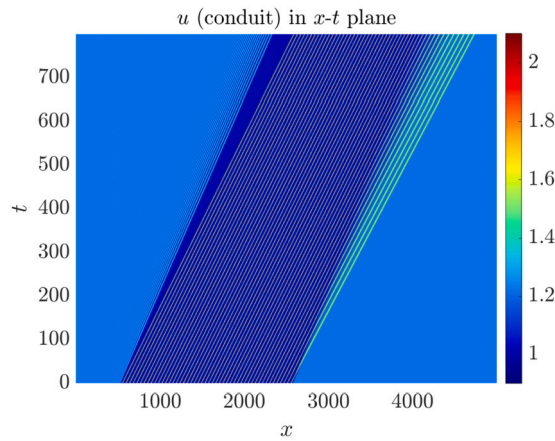


Fig. 8. The general solution structure of Cauchy problem (44) for the conduit equation is shown in  $(x, t)$ -plane. The wave train in the middle consists of 48 periodic waves, where the initial parameters for each of them are:  $u_1 = 1$ ,  $u_3 = 2$  and  $u_2 = 2 - m_0$ ,  $m_0 = 0.999$ . The wave average on the left and right of the wave train is  $\bar{u} \approx 1.216$ .

### 8. Generalized Riemann problem

We call a generalized Riemann problem (GRP) the Cauchy problem

$$u(0, x) = \begin{cases} u_L(x), & x < 0, \\ u_R(x), & x > 0, \end{cases} \tag{43}$$

where  $u_L$  and  $u_R$  are different periodic travelling wave solutions of the corresponding dispersive equations (in particular, of the conduit equation). Such a problem was studied in [11] for the Serre-Green-Naghdi and Boussinesq equations with linear dispersion, in [10] for the BBM equation, and in [31] for the fifth order KdV equation. In particular, in the first reference new stable shock-like travelling wave solutions were found linking a constant solution (denoted further by  $u_*$ ) to a periodic wave train. The shock-like transition zone between the constant state and the wave train was well described by the half of solitary wave having the wave crest at the maximum of the nearest periodic wave. Such a configuration was stable under certain conditions. For example, for the BBM equation such a shock-like structure is stable if the phase velocity of the periodic wave train is not less than the solution wave averaged representing indeed the characteristic velocity of a dispersionless homogeneous state [10]. In our case, the characteristic velocity of the dispersionless equation ( $u_t + (u^2)_x = 0$ ) is  $2u$ . Since the dispersive properties of the BBM equation are similar to those of the conduit equation, we expect that the stable configuration linking a constant state  $u_*$  to a periodic wave train having the velocity  $D$  can be also realized for  $D > 2\bar{u}$  (see the definition (35) of the wave averaged.) The aim of this section is thus to reveal the analogous solutions for the conduit equation numerically.

#### 8.1. Rankine-Hugoniot relation test

We begin by looking into a modified version of (43) in the form

$$u(0, x) = \begin{cases} \bar{u}, & x < x_0, \\ u(x), & x_0 < x < x_1, \\ \bar{u}, & x > x_1, \end{cases} \tag{44}$$

where  $u(x)$  is a wave profile that consists of  $N$  periodic waves in the interval  $(x_0, x_1)$ , and  $\bar{u}$  is the average value of a single periodic wave over a wavelength. In the numerical experiments performed here, the parameters we take for the initial periodic solution are  $u_1 = 1$ ,  $u_3 = 2$  and  $u_2 = 2 - m_0$ ,  $m_0 = 0.999$ . Then with Wolfram Mathematica, Version 12, one gets the phase speed  $D \approx 2.546$ , the average state  $\bar{u} \approx 1.216$ , and the wave length  $L \approx 42.72$ . The initial wave train is formed by introducing  $N = 48$  of such a periodic solution into one.

In Fig. 8, we show the pseudo-color plot of the solution in  $(x, t)$ -plane, observing clearly the formation of a constant state  $u_*$  on the left of the primary periodic wave train and on the right of the left rarefaction wave. This is as expected, because as in [10] we have the phase speed  $D \approx 2.546$  larger than the characteristic speed  $2\bar{u} \approx 2.432$ , a necessary condition for the existence of the stable shock-like travelling structure. The snapshot of the solution for the problem at time  $t = 600$  is shown in Fig. 9, where the solution shown on the left is obtained using the conduit equation, and on the right is obtained using the hyperbolic model. We observe good agreement of the results qualitatively.

To determine analytically the state  $u_*$ , we use the Rankine-Hugoniot relation coming from the conservative form (1) (the mass conservation law). We consider the jump relation for (1) on the travelling wave solutions for a shock having the same velocity  $D$  as

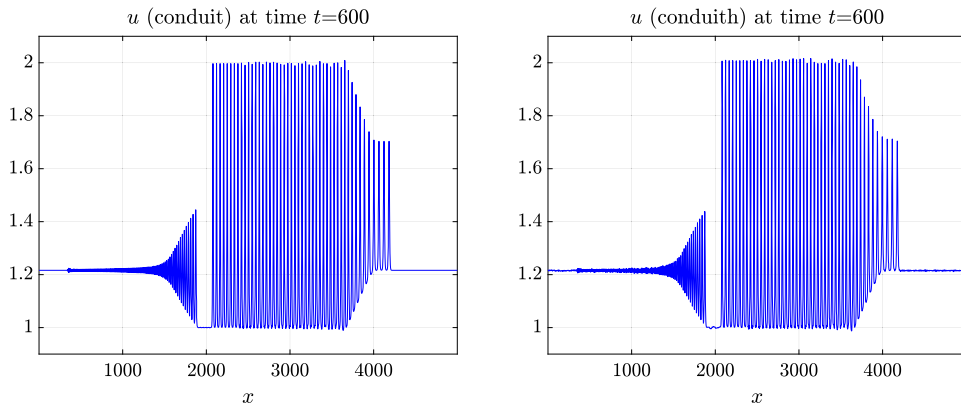


Fig. 9. The snapshot of the solution for the Cauchy problem (44) at time  $t = 600$ . The solution shown on the left is obtained using the conduit equation, and on the right is obtained using the hyperbolic model with the parameters  $c = 30$  and  $\lambda = 900$ .

that of the travelling wave train, and linking the maximum amplitude  $u_3$  of the wave train with the constant state  $u_*$  (see [11,9] for details):

$$-D(u_3 - u_*) + (u_3^2 - u_*^2 + u_3 Du''|_{u=u_3}) = 0. \tag{45}$$

We have used the fact that in the  $u_3$  state and extremal state “star” the derivative  $u'$  vanishes. The roots  $u_i$  are related by:

$$\begin{aligned} Cu_1^2 - 2u_1^2 \ln(u_1) - 2Du_1 &= Cu_2^2 - 2u_2^2 \ln(u_2) - 2Du_2 \\ &= Cu_3^2 - 2u_3^2 \ln(u_3) - 2Du_3. \end{aligned}$$

It is a system of two linear equations for  $C$  and  $D$ . If  $0 < u_1 < u_2 < u_3$ , the solution is unique. Hence, one can estimate  $Du''$  at the maximum  $u_3$  from (32):

$$Du''|_{u=u_3} = (C - 1)u_3 - 2u_3 \ln(u_3) - D. \tag{46}$$

We can now replace all into (45) to obtain the following quadratic equation for  $u_*$ :

$$-D(u_3 - u_*) + (u_3^2 - u_*^2 + u_3(Cu_3 - 2u_3 \ln(u_3) - u_3 - D)) = 0. \tag{47}$$

It has two possible solutions,  $u_*^-$  and  $u_*^+$ , with the properties  $0 < u_1 < u_*^- < u_2 < u_3$  and  $0 < u_1 < u_2 < u_*^+ < u_3$ . As in the case of the BBM equation [10], one can numerically check that only the solution  $u_*^-$  linked to the periodic wave train by jump relations is stable. In the following, this constant solution  $u_*^-$  is denoted simply  $u_*$ . The expression for  $u_*$  is quite complex, and cannot be easily analyzed analytically as for the BBM equation. So,  $u_*$  state was numerically calculated.

### 8.2. Multi-hump solitary waves

In this test problem we take the same  $u_2, u_3$ , and  $D$  as in the Cauchy problem (44), we find the value  $u_* \approx 1.000499$ . Then we may construct a multi-hump structure in the form

$$u(0, x) = \tilde{u}(x) = \begin{cases} u_*, & x < x_0, \\ u_M(x), & x_0 < x < x_1, \\ u_*, & x > x_1, \end{cases} \tag{48}$$

with  $u_M$  as a periodic wave train linked to  $u_*$ . Fig. 10, the left column, shows  $u_M$  composed of  $N = 11$  periodic wave solutions. We call this wave multi-hump solitary wave. This multi-hump solitary wave propagates stably as we can see in Fig. 11 where the snapshot solutions obtained using the conduit equation and the hyperbolic model at time  $t = 1000$  are shown. We are next concerned with a double multi-hump problem for the interaction of two multi-hump waves. The initial condition is:

$$u(0, x) = \begin{cases} \tilde{u}_L(x), & x \leq x_0, \\ \tilde{u}_R(x), & x > x_0, \end{cases} \tag{49}$$

where  $\tilde{u}_L$  and  $\tilde{u}_R$  are having analogous structure to (48), see the right column of Fig. 10 for an illustration. To be specific, for each wave train it consists of  $N = 11$  periodic waves together with a hybrid half wavelength periodic and solitary waves, and  $x_0 = 1600$ . The state values we take for  $\tilde{u}_L$  are  $u_1^L = 0.9, u_2^L = 0.907, u_3^L = 1.7$ , and that give  $D_L \approx 2.25, \bar{u}_L \approx 1.123$ , and  $u_*^L \approx 0.903477$ . For  $\tilde{u}_R$ , we have  $u_1^R = 0.9, u_2^R = 0.907, u_3^R = 1.25$ , and get  $D_R \approx 2.01871, \bar{u}_R \approx 1.00894$ , and  $u_*^R \approx 0.903467$ . Since the states  $u_*^L$  and  $u_*^R$  are approximately the same, and  $D_L > D_R$ , we can study the interaction of multi-hump solitary waves propagating on the same level  $u_*$ .

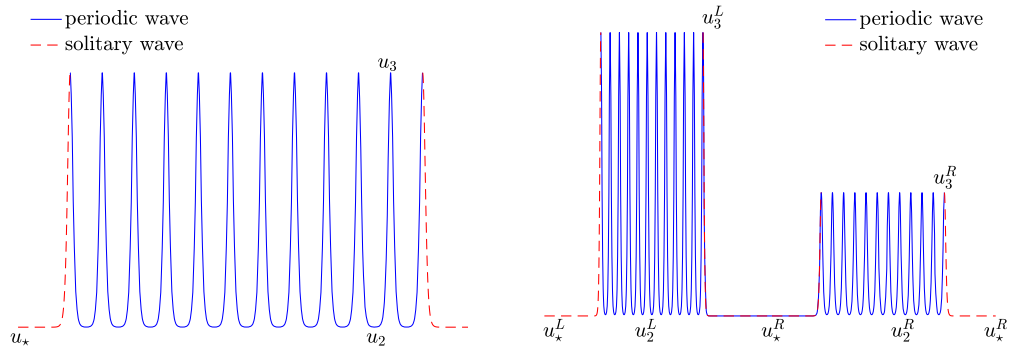


Fig. 10. Illustration of the initial conditions for the multi-hump problems. The plot shown on the left is for the single hump problem (48), and on the right is for the double hump problem (49).

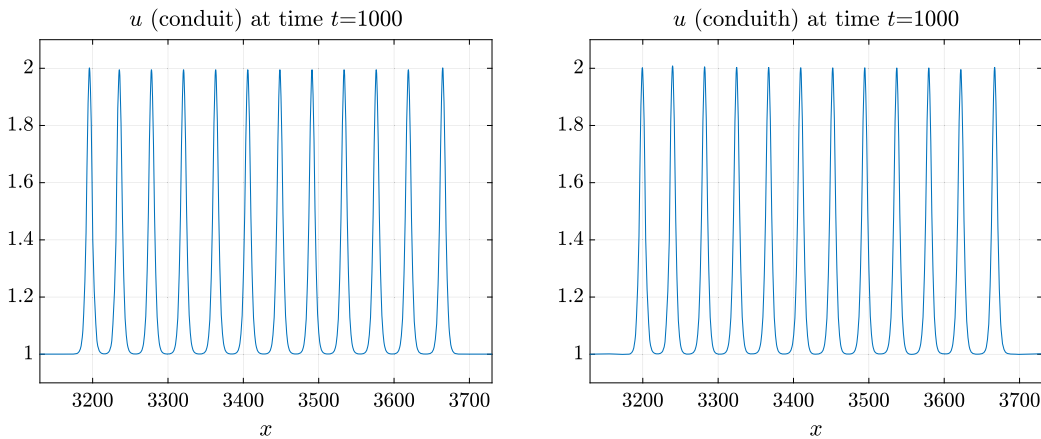


Fig. 11. The snapshot of the conduit solution for the multi-hump problem (48) at time  $t = 1000$ . The solution on the left is for the conduit equation, and on the right is for the hyperbolic model. The computation domain is  $x \in [0, 4000]$ ; only the partial solutions in the region  $x \in [3130, 3730]$  are shown.

Fig. 12 shows the numerical solutions for the conduit equation at times  $t = 500, 2000, 2500, 3000, 4000, 5000$ , observing the wave interaction, merging, and their full reconstruction. Here without introducing a large domain size, the computation domain is adjusted in time by the method to have the multi-hump solution stayed inside the region. The solutions for the hyperbolic model are shown in Fig. 13, we again observe good qualitative agreement of the solution, and the validation of the numerical solutions.

The stability of multi-hump solutions created “artificially” by combining periodic solutions and constant states related by the generalized Rankine-Hugoniot relations show that they are stable weak solutions to the conduit equation. In particular, they are stable under a “perturbation” of the conduit equation by a hyperbolic system conserving its original Godunov type form.

It would be interesting to understand whether or not the collision of multi-hump solitary waves presents a phase shift in the wave positions compared to the situation without interaction. In Fig. 14, we have shown the final positions of multi-hump solitary waves propagating with and without interaction. Numerical results show that the largest amplitude solitary wave without interaction is behind the one with interaction, while the smallest amplitude wave without interaction is in front of the one with interaction.

### 9. Conclusion

We have proposed a hyperbolic approximation of the conduit equation preserving, in particular, invariance properties of the conduit equation (reversibility in time and space) and approximating the solutions of the conduit equation with good accuracy. The advantage of the hyperbolic approximation is that it allows all the numerical tools developed for hyperbolic equation systems to be applied to the study of dispersive equations.

We have constructed new solutions to the conduit equation representing an assemblage of many waves of the same period linked to a constant solution by the generalized Rankine-Hugoniot relation, also taking into account the curvature of periodic waves. The generalized shock linking the maximum of the lateral periodic waves to a constant state has the same velocity as that of the periodic wave train. Such a multi-hump solitary wave is stable if the wave velocity is twice as great as  $\bar{u}$ . This condition means that the phase velocity of such a structure must be supercritical with respect to the homogeneous state  $\bar{u}$  having the characteristic slope  $2\bar{u}$ . The hyperbolic approximation of the conduit equation also admits such stable solutions.

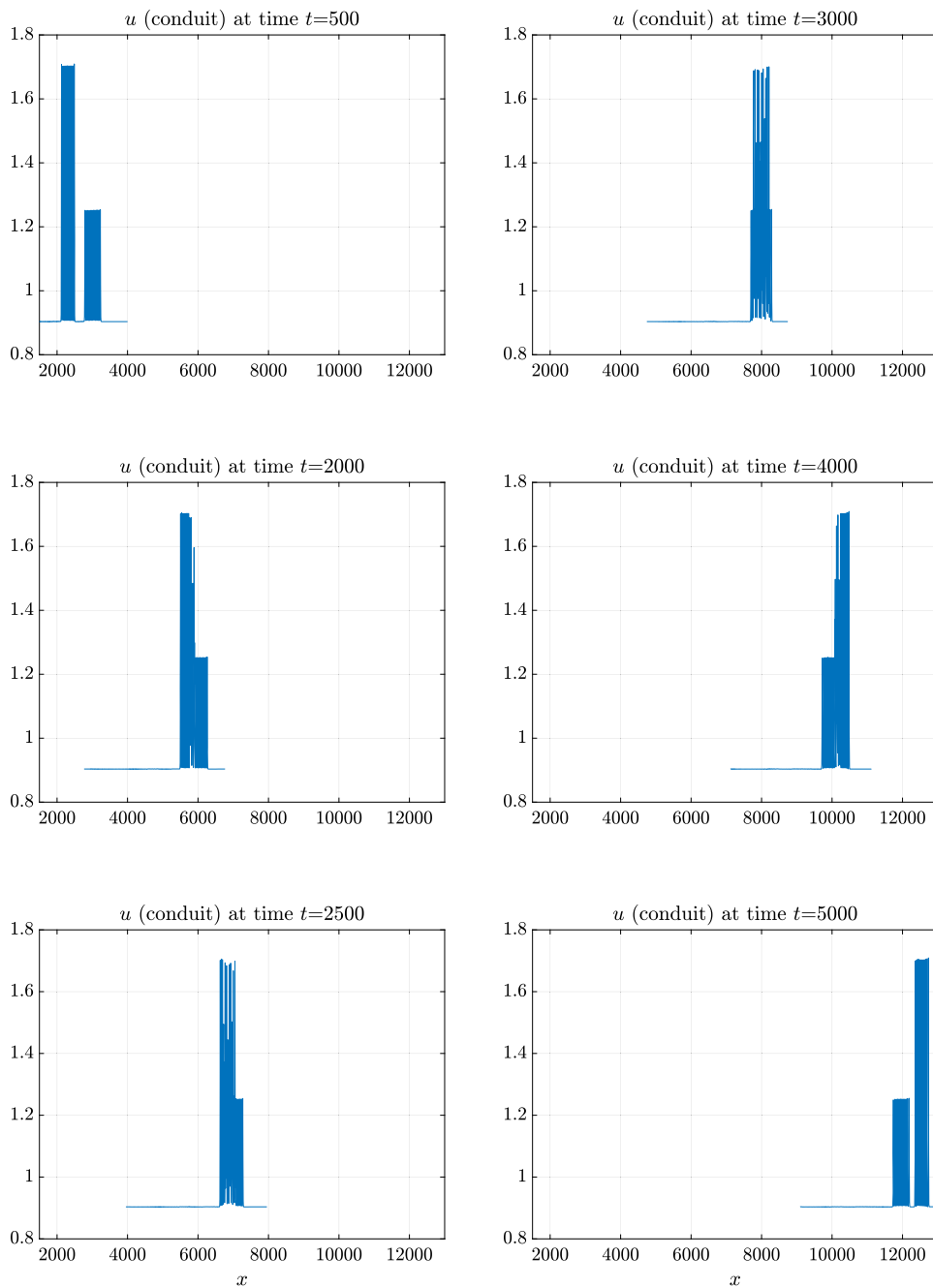


Fig. 12. The snapshot of the conduit solution for the two multi-hump problem (49) at times  $t = 500, 2000, 2500, 3000, 4000, 5000$ . The plots are displayed from the left top to bottom and continue from the right top to bottom. The computation domain is adjusted in time to have the multi-hump solution stayed in the domain; only the partial solutions in the neighborhood of the multi-hump solitons are shown.

**Ethics**

The work is original, has not been published before, and is not currently being considered for publication elsewhere.

**CRediT authorship contribution statement**

**Sergey Gavriluk:** Writing – original draft, Methodology, Investigation, Formal analysis, Conceptualization. **Boniface Nkonga:** Software, Methodology, Investigation, Formal analysis. **Keh-Ming Shyue:** Writing – original draft, Visualization, Validation, Software, Investigation, Formal analysis.

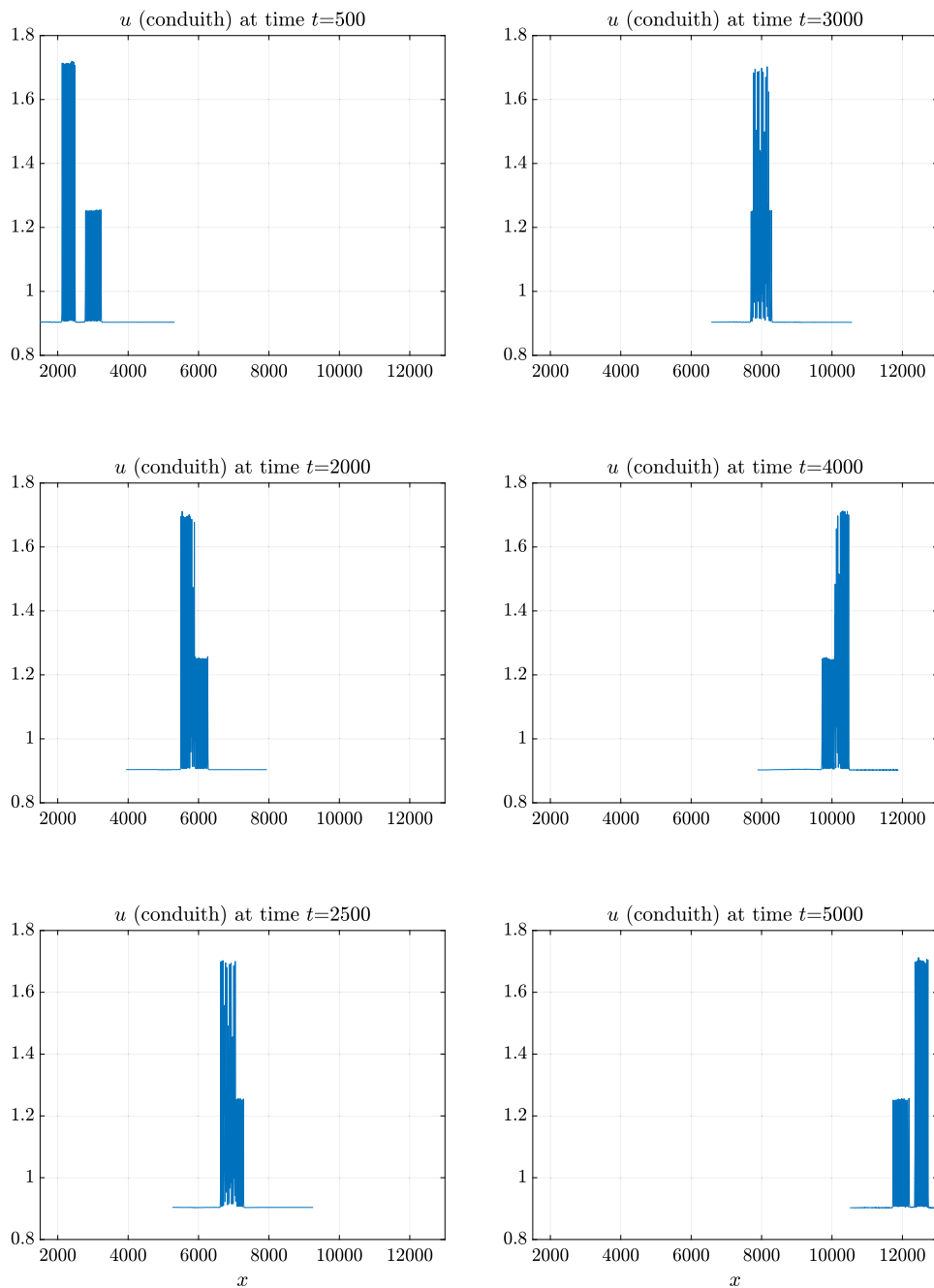


Fig. 13. The snapshot solutions of the hyperbolic conduit model for the two multi-hump problem (49) at times  $t = 500, 2000, 2500, 3000, 4000, 5000$ . The plots are displayed in the same manner as Fig. 13.

### Declaration of competing interest

The authors declare that they have no known competing financial interests or personal relationships that could have appeared to influence the work reported in this paper.

### Data availability

Data will be made available on request.

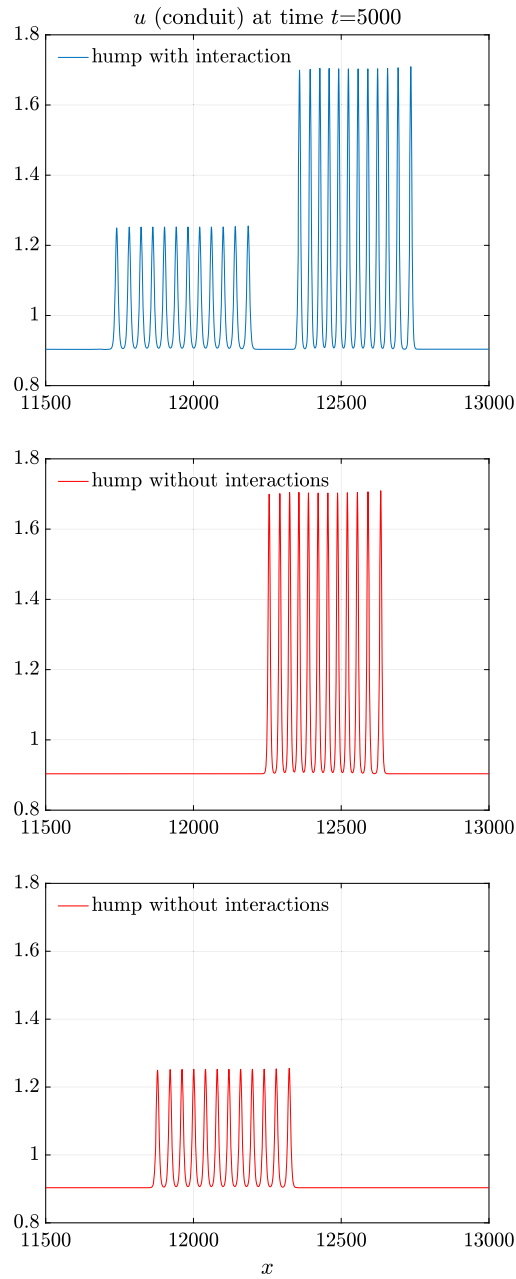


Fig. 14. The snapshot solutions of the conduit model showing the phase shift after the interaction of multi-hump solitary waves.

**Acknowledgements**

SG was partially supported by Agence Nationale de la Recherche, France (SNIP ANR-19-ASTR-0016-01). KMS thanks the Institut Mécanique et Ingénierie of Marseille and INRIA - Sophia-Antipolis - Méditerranée for financial support during his stay at IUSTI, Marseille.

**Appendix A. Numerical methods for the conduit equation**

To find approximate solutions to the conduit equation (2), we use the hyperbolic-elliptic splitting approach developed previously in [19,11,10]. This algorithm consists of two steps. In the first step, the hyperbolic step, we employ the state-of-the-art method for hyperbolic conservation laws for the numerical resolution of the equation

$$\mathcal{K}_t - (\ln u^2)_x = 0 \tag{50a}$$

over a time step  $\Delta t$ . As in [11,10], the stability condition is the CFL condition:  $\Delta t / (2\Delta x \max_i(u_i)) < 1$ , where  $u_i$  is the numerical solution in the  $i$ th grid cell. In the second step, the elliptic step, using the approximate solution  $\mathcal{K}$  computed during the hyperbolic step, we invert numerically the elliptic operator:

$$-u_{xx} + \mathcal{K}u = 1 \quad (50b)$$

for  $u$  with prescribed boundary conditions based on a finite-difference scheme [21].

It should be mentioned that from (1) one can also find numerical solutions to the conduit equation when we apply the algorithm to solve the following hyperbolic-elliptic system:

$$u_t + (u^2 + \varpi)_x = 0, \quad (51a)$$

$$-\left(\frac{\varpi_x}{u}\right)_x + \frac{\varpi}{u^2} = 2u_{xx}, \quad (51b)$$

separately for  $u$  and  $\varpi$  during each time step.

More precisely, in the hyperbolic step, we use the semi-discrete finite volume method written in a wave-propagation form as before [11], but employ a different solution reconstruction technique, the BVD (boundary variation diminishing) principle, which is more robust than the classical one for the interpolated states ( $\mathcal{K}$  for (50) or  $u$  for (51)) at cell boundaries (cf. [5] and the references cited therein). These reconstructed variables form the basis for the initial data of the Riemann problems, where the solutions of the Riemann problems are then used to construct the fluctuations in the spatial discretization that gives the right-hand side of the system of ODEs (cf. [20,17,18]). To integrate the ODE system in time, the strong stability-preserving (SSP) multistage Runge-Kutta scheme [15,30] is used. In particular, for the numerical results presented in this paper, the third-order SSP scheme was employed together with the pair of third- and fifth-order WENO (weighted essentially non-oscillatory) scheme in the BVD reconstruction process.

It is important to note that for solving the hyperbolic part of the conduit system (38a), in the MUSCL method, we used a piecewise linear reconstruction technique for approximating the spatial derivative and a second-order Heun method for the derivative in time. In the WENO3 method, we used the third-order WENO reconstruction and the third-order SSP integration in time. In the WENO5 method, we used the fifth-order WENO reconstruction and the third-order SSP integration in time as well. In the BVD35 method, as in the exact conduit equation case, we used a hybrid third- and fifth-order WENO reconstruction and a third-order SSP scheme in time. The stability condition of each of the method is the classical CFL condition.

## References

- [1] T.B. Benjamin, J.L. Bona, J.J. Mahony, Model equations for long waves in nonlinear dispersive systems, *Philos. Trans. R. Soc. Lond. Ser. A, Math. Phys. Sci.* 272 (1220) (1972) 47–78.
- [2] C. Besse, S. Gavriluk, M. Kazakova, P. Noble, Perfectly matched layers methods for mixed hyperbolic–dispersive equations, *Water Waves* 4 (3) (2022) 313–343.
- [3] S. Bourgeois, N. Favrie, B. Lombard, Dynamics of a regularized and bistable Ericksen bar using an extended Lagrangian approach, *Int. J. Solids Struct.* 207 (2020) 55–69.
- [4] S. Busto, M. Dumbser, C. Escalante, N. Favrie, S. Gavriluk, On high order ADER discontinuous Galerkin schemes for first order hyperbolic reformulations of nonlinear dispersive systems, *J. Sci. Comput.* 87 (2) (2021) 48.
- [5] X. Deng, S. Inaba, B. Xie, K.M. Shyue, F. Xiao, High fidelity discontinuity-resolving reconstruction for compressible multiphase flows with moving interfaces, *J. Comput. Phys.* 371 (2017) 945–966.
- [6] F. Dhaouadi, N. Favrie, S. Gavriluk, Extended Lagrangian approach for the defocusing nonlinear Schrödinger equation, *Stud. Appl. Math.* 142 (3) (2019) 336–358.
- [7] V. Duchêne, Rigorous justification of the Favrie–Gavriluk approximation to the Serre–Green–Naghdi model, *Nonlinearity* 32 (2019) 3772–3797.
- [8] N. Favrie, S. Gavriluk, A rapid numerical method for solving Serre–Green–Naghdi equations describing long free surface gravity waves, *Nonlinearity* 30 (7) (2017) 2718.
- [9] S. Gavriluk, K.M. Shyue, Singular solutions of the BBM equation: analytical and numerical study, *Nonlinearity* 35 (1) (2021) 388.
- [10] S. Gavriluk, K.M. Shyue, Hyperbolic approximation of the BBM equation, *Nonlinearity* 35 (3) (2022) 1447.
- [11] S.L. Gavriluk, B. Nkonga, K.M. Shyue, L. Truskinovsky, Stationary shock-like transition fronts in dispersive systems, *Nonlinearity* 33 (2020) 5477–5509.
- [12] S.L. Gavriluk, S.M. Shugrin, Media with equations of state that depend on derivatives, *J. Appl. Mech. Tech. Phys.* 37 (1996) 177–189.
- [13] S.K. Godunov, An interesting class of quasi-linear systems, *Dokl. Akad. Nauk SSSR* 139 (3) (1961) 521–523.
- [14] S.K. Godunov, E. Romenskii, *Elements of Continuum Mechanics and Conservation Laws*, Springer US, 2003.
- [15] S. Gottlieb, C.W. Shu, E. Tadmor, Strong stability–preserving high–order time discretization methods, *SIAM Rev.* 43 (2001) 89–112.
- [16] M.A. Johnson, W.R. Perkins, Modulational instability of viscous fluid conduit periodic waves, *SIAM J. Math. Anal.* 52 (1) (2020).
- [17] D.I. Ketcheson, R. LeVeque, Wenoclaw: a higher order wave propagation method, in: *Hyperbolic Problems: Theory, Numerics, Applications*, IMA J. Appl. Math. (2005) 609–616.
- [18] D.I. Ketcheson, M. Parsani, R. LeVeque, High-order wave propagation algorithm for hyperbolic systems, *SIAM J. Sci. Comput.* 35 (1) (2013) A351–A377.
- [19] O. Le Métayer, S. Gavriluk, S. Hank, A numerical scheme for the Green–Naghdi model, *J. Comp. Physiol.* 229 (2010) 2034–2045.
- [20] R.J. LeVeque, *Finite Volume Methods for Hyperbolic Problems*, Cambridge University Press, 2002.
- [21] R.J. LeVeque, *Finite Difference Methods for Ordinary and Partial Differential Equations: Steady-State and Time-Dependent Problems*, SIAM, Philadelphia, 2007.
- [22] N.K. Lowman, M.A. Hoefel, Dispersive hydrodynamics in viscous fluid conduits, *Phys. Rev. E* 88 (2013) 023016.
- [23] N.K. Lowman, M.A. Hoefel, Dispersive shock waves in viscously deformable media, *J. Fluid Mech.* 718 (2013) 524–557.
- [24] N.K. Lowman, M.A. Hoefel, G.A. El, Interactions of large amplitude solitary waves in viscous fluid conduits, *J. Fluid Mech.* 750 (2014) 372–384.
- [25] M.D. Maiden, N.A. Franco, E.G. Webb, G.A. El, M.A. Hoefel, Solitary wave fission of a large disturbance in a viscous fluid conduit, *J. Fluid Mech.* 883 (2020) A10.
- [26] M.D. Maiden, M.A. Hoefel, Modulations of viscous fluid conduit periodic waves, *Proc. R. Soc. A* 472 (2016) 20160533.
- [27] M.D. Maiden, N.K. Lowman, D.V. Anderson, M.E. Schubert, M.A. Hoefel, Observation of dispersive shock waves, solitons, and their interactions in viscous fluid conduits, *Phys. Rev. Lett.* 116 (2016) 174501.
- [28] J. Nocedal, S.J. Wright, *Numerical Optimization*, second edition, Springer, 2006.

- [29] P. Olson, U. Christensen, Solitary wave propagation in a fluid conduit within a viscous matrix, *J. Geophys. Res.* 91 (1986) 6367–6374.
- [30] C.W. Shu, High order weighted essentially nonoscillatory schemes for convection dominated problems, *SIAM Rev.* 5 (2009) 82–126.
- [31] P. Sprenger, M.A. Hoefer, Discontinuous shock solutions of the Whitham modulation equations as dispersionless limits of travelling waves, *Nonlinearity* 33 (2020) 3268–3302.
- [32] S. Tkachenko, S. Gavrilyuk, J. Massoni, Extended Lagrangian approach for the numerical study of multi-dimensional dispersive waves: applications to the Serre–Green–Naghdi equations, *J. Comput. Phys.* 477 (2023) 111901.